Revision 1

Word Count: 5404

Biological control of ultra-skeleton mineralization in coral

Miaohong He, * Wenfeng Deng, Xuefei Chen, Yanqiang Zhang, Gangjian Wei

State Key Laboratory of Isotope Geochemistry, CAS Center for Excellence in Deep Earth Science, Guangzhou Institute of Geochemistry, Chinese Academy of Sciences, Guangzhou 510640, China

*Corresponding author: Miaohong He
Tel: 86-20-85290501
E-mail: mhhe@gig.ac.cn

Abstract

Understanding the mineralization of coral is significant for the formation of coral reefs and paleoclimatic reconstructions. However, the fundamental mechanisms involved in biomineralization are poorly understood. A combination of Raman spectral and cross-polarized reflected light microscopy imaging was used to examine the three-dimensional spatial distribution of the skeletal ultrastructures and their associated mineral, organic, water chemistry in coral, which enable insight into the spatial growth features of the ultrastructures and possible formation processes. A possible mechanism is proposed whereby biological control the formation of skeletal ultrastructures, which likely involves compartmentalized calcifying cells and their related cellular activities. This could clarify the association between coral skeletal mineralization and biology, and may be beneficial to better protection and application of coral reefs.

Keywords: Coral; skeletal ultrastructure; calcifying cells; three-dimensional distribution; mineralization mechanism

Introduction

Biomineralization results in the Earth's spectacular coral reefs and forms high-resolution archives of past environmental change (Cohen and McConnaughey 2003; Meibom et al. 2003; Otter 2019). Mineralization by coral has significance for geochemistry, climatology, and biology (DeCarlo et al. 2019a; McCulloch et al. 2012; Motai et al. 2012), and a better understanding of the biology of coral skeletogenesis might provide new insight into reef growth patterns (Cuif and Dauphin 2005a; DeCarlo et al. 2019b; Meibom et al. 2003), future responses of coral reefs to environmental change (Cohen et al. 2009a; Farfan et al. 2018a; Georgiou et al. 2015; Hennige et al. 2015; Meibom et al. 2006), and quantitative paleoenvironmental proxies (Chen et al. 2015; Meibom et al. 2007; Thompson 2022).

Despite the widespread significance of coral mineralization and extensive investigations (Cusack and Freer 2008; DeCarlo et al. 2019a; Mann 2001; Meldrum 2003), the fundamental mechanisms of mineralization remain poorly understood (Allemand et al. 2011). Several models of coral mineralization have been proposed, including diurnal growth (Cohen et al. 2001; Gladfelter 1983a), the organic template/envelope (Constantz 1986; Cuif et al. 2003; Tissier 1988), growth related to amorphous calcium carbonate (Mass et al. 2017; Von Euw et al. 2017), cyclical changes in the saturation state of calcifying fluids (Al-Horani et al. 2003; Holcomb et al. 2009), and control by different calcifying cells (Cuif and Dauphin 1998; Meibom et al. 2008). However, these hypotheses are based on either the skeletal chemistry (elemental, isotopic, and organic) or crystalline morphologies, and have not considered the spatial growth features (i.e., the various orientations) of ultrastructures.

Understanding the biological controls on the coral mineralization requires a robust knowledge of coral ultrastructures and growth (Gilis et al. 2015; Otter 2019; Stolarski 2003). The coral skeleton consists primarily of two ultrastructures, which are centers of calcification (COC) and fibers (Cohen and Thorrold 2007; Cusack and Freer 2008; Meibom et al. 2008). The former accounts for only ~3% of the entire skeletal weight, is embedded within the fibers (i.e., the host medium), and has an important role in skeletal formation (Allison 1996; Cuif and Dauphin 1998). The longitudinal and lateral extensions of the COC determine the overall architecture of the coral skeleton (Cuif and Dauphin 1998; Meibom et al. 2006; Sugiura et al. 2021). Moreover, the COC are generally considered to be nucleation sites for fiber crystallization (Cohen and McConnaughey 2003; Cohen et al. 2001; Constantz 1986). Therefore, the COC are fundamental to coral skeletogenesis (Cohen et al. 2001; Constantz 1986).

Investigating the nature, growth, and chemistry of the COC is challenging because of their small diameter (generally <10 μm) and concealed occurrence (Cuif and Dauphin 2005b; Cuif et al. 2003; Meibom et al. 2006). Conventional physical separation followed

by solution-based analyses, and even microanalysis by laser ablation–inductively coupled plasma–mass spectrometry and secondary ion mass spectrometry, are unable to analyze the COC without contamination from adjacent fiber materials (Chen et al. 2020; Cuif and Dauphin 1998; Meibom et al. 2003). A limited number of previous studies have focused on identifying the distinctions between the COC and fibers in terms of either their crystalline morphology (Cuif and Dauphin 1998; Motai et al. 2012), organic phase (Cuif et al. 2003; DeCarlo et al. 2018), or elemental and isotopic compositions (Cuif and Dauphin 1998; Holcomb et al. 2009). However, few studies have examined the distribution of the COC, particularly within the three-dimensional coral skeleton, which might provide insights into the formation of ultrastructures and biological effects on mineralization (Meibom et al. 2007; Stolarski 2003).

In this study, the spatial variations in coral skeleton chemistry and ultrastructures were investigated with high spatial-resolution confocal laser Raman spectroscopy and optical microscopy in two- and three-dimension. The former technique, having been successfully used to reveal mineralogical and crystallographic characterization of carbonates (DeCarlo 2018; DeCarlo et al. 2017; Farfan et al. 2022; Farfan et al. 2018b; Higuchi et al. 2014; Urmos et al. 1991) and to reconstruct coral skeletal fiber arrangement and growth (Wall and Nehrke 2012; Zhang et al. 2011), enables to constrain the spatial variations in chemistry, including water, organics, mineral phases, and ultrastructures of skeleton. These techniques provide new insights into the biological mechanisms responsible for the formation of coral skeletons.

Experiment methods

Sample preparation

Three samples of the zooxanthellate coral *Porites* sp. were collected from a depth of 4 m on the Luhuitou fringing reef of Hainan Island in the northern South China Sea (18°12.87′ N, 109°28.47′ E) in April 2010 (Zou et al. 2021). The samples were prepared

as shown in Fig. 1a and described previously (Zou et al. 2021). The specimen was sliced parallel to the axis of maximum skeletal growth into a slab that was ~3 mm thick. The slab was mounted in epoxy resin, further cut into a slice that was ~1 mm thick, and then manually polished with a fine diamond disk under flowing water to a ~100-μm-thick slice. The effect from the chosen solvent might not be excludable but it is still minor on surface ultrastructures, and insusceptible on the inner ultrastructures. The final polishing step (using monocrystalline diamond suspension with size of 1 μm (MetaDi, USA)) was carefully monitored to ensure the COC were exposed. The slice was then mounted in new epoxy resin, ultrasonically cleaned with deionized water, and dried (50ºC) prior to analysis.

Instrumental and analytical procedures

A confocal Raman microscope (WITec Alpha-300R; Ulm, Germany) equipped with a 488 nm excitation laser and Zeiss 50× objective lens was used for the Raman spectroscopic analyses at the State Key Laboratory of Isotope Geochemistry, Guangzhou Institute of Geochemistry, Chinese Academy of Sciences (SKLaBIG-CAS), Guangzhou, China. Measurements were undertaken at room temperature, with a laser power of 30 mW and over a wavenumber range of 80–4000 cm^{-1}.

The Raman spectra imaging procedures are summarized in Fig. 1b. The coral was placed on an *x*–*y* stage. Laser scans in the lateral plane involved an array of 85 × 125 spots analyses with a 1 μm step size and 1 s integration time, which covered an imaging area of 85 × 125 μm. For the three-dimensional imaging, the incident laser was focused deeper into the sample to acquire an image stack with a *z* (depth) step size of 2 μm. This avoids interference from layers at different depths, because the step size is much greater than the depth resolution of the laser (~1 μm) (Dieing et al. 2011). The imaged volume was 85 × 125 × 14 μm, with seven layers in the *z* direction. The average integrated intensity decreases with depth (Dieing et al. 2011), and thus intensity corrections were

applied to the spectral datasets for each layer. Data were processed using a self-developed LabView program, and the two- and three-dimensional images were constructed from three-dimensional data (*x* and *y*, and the integrated Raman band intensity of interest) and four-dimensional data (*x*, *y*, and 5*z*, where *z* was magnified by a factor of 5 to display the depth profile more clearly, and the integrated Raman band intensity of interest), using Surfer and Voxler software, respectively (He et al. 2017; Huang et al. 2011).

The coral skeleton was also examined with an optical microscope (Leica, DM2700M) under cross-polarized reflected light (CPRL), which is a previously unreported analysis mode, at the SKLaBIG-CAS. In addition, the secondary layer of skeleton (different depth layer) instead of superficial one was subjected to CPRL microscopy imaging based on the transparent and nearly colorless nature of the epoxy resin in CPRL images.

Results

Raman analyses of the coral skeletal ultrastructures

Typical Raman spectra of skeletal COC and fibers are shown in Fig. 2. The remarkable difference in composition between these ultrastructures is the organic matrix (OM; with sp^3 CH_x stretching modes at 2850–3000 cm^{-1}) (DeCarlo et al. 2018; Von Euw et al. 2017), which occurs only in the COC (Figs. 2c, and f). The carbonate-related Raman bands (lattice modes at 153 and 217 cm^{-1}; ν_4 planar bending of C–O at 705 cm^{-1}; ν_1 symmetric stretching of CO_3^{2-} units at 1085 cm^{-1}) (Farfan et al. 2021; Urmos et al. 1991) and water-related Raman bands (O–H stretching mode at 3000–3750 cm^{-1}) (Hild et al. 2008) characterize both the COC and fibers, but with clear intensity differences. The broad O–H stretching band (Figs. 2c, f) was assigned to inorganic water rather than an organic phase containing OH, as no Raman bands of organic groups were simultaneously determined in the fibers, even though the O–H stretching band was much stronger in intensity than for the COC. The Raman bands at 153, 217, 705, 1085, 2910, and 3410 cm^{-1} can distinguish the COC from the surrounding fibers.

Fig. 3a and supplementary Figs. 2g–3g show reflected light microscopic images of the coral skeleton in two contrasting color regions, where the COC are darker than the fibers. The optical differences between these two structures have been documented in earlier studies (DeCarlo et al. 2018). The two-dimensional Raman images, based on the area integration of Raman bands of interest (carbonate, water, and organics), are shown in Figs. 3b–g and supplementary Figs. 1b–e, and are consistent with the optical image and provide better defined boundaries between the COC and fibers than routine light microscopic approach. This verifies that Raman spectral imaging can distinguish between these two structures. The tentacle-like, blue–purple region in the images (Figs. 3b–f, and supplementary Fig. 1b–d), with consistently weaker mineral- and water-related bands but stronger organic-related bands (Fig. 3g and supplementary Fig. 1e), correspond to the darker region in the microscopic image (Fig. 3a and supplementary Fig. 1a) and the COC.

Two-dimensional imaging can reveal the ultrastructural and chemical variation of the processed surface of the coral skeleton. However, there may be further information that can be obtained from beneath the coral surface. There are a range of conflicting hypotheses regarding the shape, growth, and arrangement of the COC (Cohen and McConnaughey 2003; Cohen et al. 2001; Cuif and Dauphin 1998). To investigate these, three-dimensional Raman spectral imaging was applied to the coral sample.

The three-dimensional distribution of Raman bands within the studied volume of the coral skeletons are portrayed in Figs. 4a–f and supplementary Figs. 2, 3a–f, and reveal details of the intraskeletal spatial distributions of components (mineralogical, organics, and water) and ultrastructures that were not evident from surface observations. The largest COC in the imaged volume is the same as that observed in the two-dimensional images (Fig. 3 and supplementary Fig. 1), with an actual diameter that extended ~40 μm into the skeleton (Fig. 4), which is considerably larger than that generally thought to characterize reef-building corals (5–10 μm) (Cuif and Dauphin 2005b; Cuif et al. 2003; Meibom et al. 2006). In addition, there are multiple parallel/or radiating COC columns

that were separated from each other (Fig. 4 and supplementary Figs. 2–3), which were not observable in previous studies (Cuif and Dauphin 2005b; Meibom et al. 2008; Von Euw et al. 2017). This indicates that there is more than one COC column at different depths in an individual coral skeleton, which could be further ascertained by three-dimensional FIB-SEM (Focused Ion Beam-Scanning Electron Microscope) rendition (supplementary Fig. 5). Skeletal COC structures have lower water and mineral contents than the fibers, both on the coral surface and in its interior. Organic compounds have higher concentrations in the COC, but these are restricted to specific depths and are not uniform throughout the COC (Fig. 4f and supplementary Figs. 2–3f).

Cross-polarized reflected light microscopy imaging of coral skeletal ultrastructures

Cross-polarized light microscopy (CPL) imaging in transmitted light has been frequently used for mineral identification (Von Euw et al. 2017). The COC and fibers in thin-sectioned coral skeleton have also been examined with this approach and shown to have distinct interference colors (Motai et al. 2012; Von Euw et al. 2017). However, such analysis requires very thin samples (4–5 μm)(Cuif and Dauphin 2005a), which are challenging to prepare and would modify or severely damage the distribution of the COC. Moreover, images obtained using this approach are ambiguous because of the interference of transmitted light from within the object volume, which makes it difficult to resolve details within the object volume (Risk and Pearce 1992).

In contrast to conventional CPL microscopy imaging (Von Euw et al. 2017), the newly developed cross-polarized light microscopy imaging in reflected light (CPRL) approach (first used herein) yields exquisite images of fine textural features of the COC, which are less sensitive to sample thickness. This benefits from the different light transparency and colors of the COC and fibers, with the former appearing opaque and white, and the latter being transparent and nearly colorless. These distinct optical properties might be due to compositional (e.g., organic phases), porosity, or crystal morphological differences (e.g.,

205 elongated, acicular, and regular crystals with sizes of > 1 μm in the fibers, and fusiform,
206 granular, randomly oriented, and nano-sized crystals in the COC) (Cohen et al. 2001;
207 Holcomb et al. 2009). This makes it possible to distinguish the embedded micron-sized
208 COC structure from the bulk fibers, and to determine the distribution and shapes of the
209 COC in the coral skeleton.

210 The sample subjected to Raman imaging was also used for CPRL microscopy imaging,
211 and the images revealed a distribution of the COC similar to that in the Raman images
212 (Figs. 3–5 and supplementary Figs. 1–3), but also contained more detailed information on
213 the distribution and shapes of the COC within the deeper coral skeleton. As such, the
214 CPRL microscopy imaging is a powerful and rapid method for visualizing the
215 three-dimensional spatial distribution of ultrastructures in coral skeletons.

216 The aforementioned results focused on the superficial skeleton, and its ultrastructure
217 would have been modified by sample preparation, especially the slicing and polishing. To
218 acquire robust observations of the COC, the underlying layers were investigated by
219 simply adjusting the focal length of the optical microscope. This revealed multiple COC
220 with a regular arrangement in the form of either parallel or radiating clusters. Each COC
221 column comprised alternating relatively long–thin filaments and short–thick nodules
222 (Figs. 5c–h, and supplementary Fig. 4d–f). At high magnification (Figs. 5e, h, and
223 supplementary Fig. 3f), the individual COC columns appear to increasingly branch into
224 more filaments and nodules with increasing skeletal extension. Some fractures (Fig. 5)
225 occur at both the superficial and secondary layered skeletons.

226

227 **Discussion**

228 **Chemical features of the skeletal ultrastructures**

229 The consistently strong Raman band at 217 cm^{-1} (typical of aragonite and distinct from
230 calcite at 277 cm^{-1}) in both the COC and fibers demonstrates that aragonite is the
231 dominant mineral in both COC and fiber (Weiner et al. 2003). Although tiny calcite or

amorphous calcium carbonate (ACC) had been previously reported to occur in bio-skeletons (Constantz and Meike 1989; Otter et al. 2019; Von Euw et al. 2017; Weiner et al. 2003), the neither calcite associated peak nor peak broadening or shift of the 1087 cm^{-1} band that is typical of ACC, were observed (Figs. 2b, e). Nevertheless, this might not completely preclude their presence, because ACC might have been a short-lived transient phase (i.e., for several hours) or occurred only in the nascent coral skeleton or tissue rather than the adult skeleton (Akiva et al. 2018; Mass et al. 2017), on the other hand, the possible small sized other forms of crystals could not be resolved by the resolution of Raman (Boon et al. 2020). Despite aragonite being found in both COC and fibers, these two ultrastructures are still distinguishable due to the differences in crystallinity, crystal disorder, and impurities (Cohen et al. 2001; Cuif and Dauphin 1998; Holcomb et al. 2009; Mass et al. 2017). Therefore, Raman mapping is a useful tool to reveal the microstructural nature of the coral skeleton.

The organic matrix was previously considered to be key in the process of biomineralization (Cusack and Freer 2008). However, numerous uncertainties remain with respect to the role of the organic matrix during skeletogenesis, including whether it acts as the framework or controls crystal mineralogy, orientation, and growth (Cuif and Dauphin 2005a; DeCarlo et al. 2018; Mann 2001). The distribution of organic material is strongly coupled with the skeletal ultrastructures, particularly the higher concentrations in the COC (Figs. 3g, 4f, supplementary Figs. 1e, 2f, and 3f), which is in agreement with previous studies (Cuif et al. 2003; DeCarlo et al. 2018; Meibom et al. 2007). Almost no measurable signal of organic material was detected by the Raman analyses of the fibers, which might be due to the amounts being below the detection limit or differences in the origins, form, nature and composition of the organic material (Allemand et al. 2011; Cohen and McConnaughey 2003; DeCarlo et al. 2018; Falini et al. 2015).

Unexpectedly, the three-dimensional spatial distribution of the organic matrix is restricted to a certain depth in the COC rather than being uniformly dispersed throughout

the entire COC (Fig. 4f and supplementary Figs. 2f–3f). This suggests that formation of the COC is not due to the organic template/envelope model as previously proposed (Cuif and Dauphin 2005a; Tissier 1988). Since the former model describes initial deposition of organic material that become a template for the adsorption of precursor ions and subsequent crystallization, which means the resultant organic compounds should be uniformly dispersed in the COC; while the latter one (organic envelope) should cause the organic compounds to be arranged in a cortex surrounding the COC (Tambutté et al. 2011; Tissier 1988). However, these features were not observed.

The water enrichment (Figs. 3f, 4e, supplementary Figs. 1d, 2e, and 3e) at the coral surface and in its interior precludes the possibility of this being an artefact caused by sample preparation as, if this were the case, the water should be concentrated on the skeletal surface due to adsorption. A plausible explanation is that the coral skeleton consists of aragonite crystals and hydrated organic matrix (Cuif and Dauphin 1998; Gaffey 1988; Holcomb et al. 2009), which is consistent with general biochemical characterizations (Dauphin 2001; Yan et al. 2020), and thermogravimetric analysis of coral skeletons that recorded simultaneous weight loss of water and associated organic compounds (CO_2) (Cuif et al. 2004). However, the hydrated nature of the organic matrix cannot solely account for the observed water distribution between the COC and fibers, as the fibers are water-rich and organic-poor as compared with the COC. Therefore, some other factors, such as small inclusions or the hydrophobic nature of the organic compounds, may be significant (Cuif and Dauphin 2005a; Falini et al. 2015; Gaffey 1988).

Growth features of the skeletal ultrastructures

The skeletal COC growth features have various orientations, including transverse and longitudinal, and can be observed by the three-dimensional imaging. A striking feature of the COC is their periodic and continuous growth. In CPRL microscopy images (Fig. 5

and supplementary Figs. 2–4), there are highly regular, micron-scale alternations of nodules connected by thin filaments. Additionally, adjacent COC columns form parallel /or radiating clusters that correspond to successive growth steps of the COC. Each periodic step corresponds to a length of 50–58 μm, which possibly reflects a daily growth increment, based on the average linear extension rate of this coral (~50 μm/d) (Zou et al. 2021). The nodules and filaments could correspond to nighttime and daytime growth, respectively, given that enhanced organic deposition would occur under the lower-pH condition, and lower extension rate at nighttime as compared with daytime (Domart-Coulon et al. 2014; Tambutté et al. 2015).

Previous studies have suggested that the COC only form at night and undergo discrete growth, based on observations of skeletal morphologies (Cohen et al. 2001; Gladfelter 1983a), but this conclusion was likely drawn based on observations of the visible and relatively large nodules, whereas the daytime-deposited filament-shaped COC connecting the nodules were not observed. To our knowledge, the daily growth increments preserved in the COC have not been previously reported. The differences in diurnal mineralization may be linked to diurnal changes in environmental or physiological factors. For example, the lower nighttime reef-flat temperature and interruption of photosynthesis would reduce CO_3^{2-} concentrations, resulting in diurnal differences in growth kinetics (Constantz 1986; DeCarlo et al. 2019b). In addition, cells and polyps are known to undergo biological diurnal growth variations, such as tissue expansion–contraction (Raz-Bahat et al. 2006), changes in the shapes of cell layers (Barnes and Yonge 1972), and cell division (Gladfelter 1983b). The diurnal growth increments recorded in the COC highlights their potential use for higher temporal resolution geochronology than conventional radiographic techniques (i.e., skeleton densities) that record annual or seasonal events (Stolarski 2003).

The continuous growth of the COC except in some fractures and its diurnal growth patterns could preclude the prevailing diurnal model as the skeletogenesis of COC and

313 fibers, which considered that the formations of the COC and fibers are temporally
314 decoupled, involved initial deposition of the COC in the form of fusiform crystals at
315 night, and subsequent development of needle-like crystal fibers on COC nucleation sites
316 during the day (Cohen et al. 2001; Gladfelter 1982; Gladfelter 1983a). If such diurnal
317 growth actually occurs, then the nighttime-deposited COC would be subsequently
318 covered by daytime-deposited fibers in both the transverse and longitudinal growth
319 directions, which would form discontinuous COC with each discrete length interval
320 defining the nighttime growth. But such case has not been observed, implying that COC
321 may be deposited during both daytime and nighttime, and that their extension rate is
322 similar to or higher than that of the fibers. This has been verified together by
323 Domart-Coulon et al. (Domart-Coulon et al. 2014) and Raz-Bahat et al. (Raz-Bahat et al.
324 2006) based on *in situ* skeletal labeling culture experiments. Furthermore, the
325 arrangement of multiple COC columns (labeled in Figs. 4–5 and supplementary Figs. 2–4)
326 with quasi-parallel or radiating growth characteristics in defined positions within the
327 skeleton is inconsistent with a cyclical process driven by changes in the saturation state of
328 the calcifying fluid (Holcomb et al. 2009). Such inorganic processes would make the
329 distribution of the COC discontinuous and random, as in the case of fluid-filled cavities
330 produced by inorganic crystallization (Gladfelter 1982), rather than observed patterns. In
331 addition, these two structures have different biochemical properties, such as organic
332 contents, indicating deposition by different biological controls.
333
334 **Coral biomineralization by compartmentalized calcifying cells**
335 According to the upper discussion, the prevalent mineralization models for coral
336 including diurnal growth (Cohen et al. 2001; Gladfelter 1983a), the organic
337 template/envelope (Constantz 1986; Cuif et al. 2003; Tissier 1988), growth related to
338 amorphous calcium carbonate (Mass et al. 2017; Von Euw et al. 2017), cyclical changes
339 in the saturation state of calcifying fluids (Holcomb et al. 2009) could be precluded, and

the most likely mineralization of coral skeleton microstructures is a biologically controlled process, both spatially and temporally.

The COC columns begin with a single or few nodules and filaments, and subsequently branch with increasing skeletal growth (Fig. 5 and supplementary Figs. 2–4). Although it is difficult to quantitatively count the thin and intricate filaments, each nodule appears to be able to divide into two, even though some quasi-parallel or radiating COC columns do not perfectly match this pattern. Such pattern of COC seems to correspond to cell division which coincidently occurs on a daily cycle (Gladfelter 1983b; Lecointe et al. 2013). Combination with the fine arrangements of ultrastructures (e.g., the distance (≤10 μm) between adjacent COC columns analogous to the size of calcifying cell within an individual skeleton (Domart-Coulon Isabelle et al. 2001; Mass et al. 2012), COC branches with period of day consistent with cell division (Gladfelter 1983b; Lecointe et al. 2013), and organic-rich, might imply the formation of solitary nodules or filaments is likely controlled by a single cell. And multiple cells without complete separation are responsible for the overlapping of multiple secretory nodules or filaments. Furthermore, the multiple, parallel/ or radiating COC columns are isolated from each other during growth of the skeleton, suggesting that precisely calcifying cells that are fixed relative to the skeleton form this rigorous three-dimensional architecture. More importantly, cell coordination during skeletogenesis is required, which is consistent with previous suggestions that crystal growth does not occur in individual coral cells, but occurs in multicellular isolates (Domart-Coulon Isabelle et al. 2001; Mass et al. 2012). This is because cell viability and functionality should be preserved by cell-to-cell contacts and interactions (Meibom et al. 2007).

This hypothesis may be further supported by the histology of the skeleton–tissue interface, which indicates the coral skeletons are in tight and direct physical contact with a calcifying cell layer without a visible calcifying fluid layer (Clode and Marshall 2003; Raz-Bahat et al. 2006; Tambutté et al. 2007). The physical closeness of the cell with the

underlying skeleton is considered to be an indication of its level of involvement in skeletogenesis (Cohen and McConnaughey 2003). In additional, cells overlying the skeleton form a single layer of at least two types, based on cell shapes and activities (Clode and Marshall 2002; Tambutté et al. 2007), and the cell distribution and density vary spatially and temporally during skeletal growth (Tambutté et al. 2007). Domart-Coulon et al. (Domart-Coulon Isabelle et al. 2001) suggested that isolated cells enable *in vitro* crystallization of aragonite independent of the coral skeleton as a substrate. This demonstrates that, at a cellular level, mineralization can still occur without a fluid layer between the calcifying cells and skeleton. In summary, previous studies, combined with the spatial distribution of ultrastructures and chemistry documented in this study, suggest that coral skeletogenesis is likely controlled by compartmentalized calcifying cells.

A possible model for coral skeletogenesis by compartmentalized calcifying cells is summarized in Fig. 6. This model is inferred based on data from the present and previous studies (Brahmi et al. 2010; Cuif and Dauphin 2005b; Mass et al. 2012; Meibom et al. 2008). Three possible successive stages are proposed to be involved: (*i*) attachment of special calcifying cells; (*ii*) diurnal secretion by the cells; (*iii*) cell proliferation that induces branching of the COC.

In the first stage, the calcifying cells may adhere to the surface of the base (the previous skeleton) by attaching to highly specialized points. These settling cells might be divided into two types, which are assumed to be round- and spindle-shaped cells based on their appearances as identified in histological observations (Clode and Marshall 2002; Domart-Coulon Isabelle et al. 2001; Tambutté et al. 2007), which could be exemplified from Fig. 4 in the previous study of the tissue-skeleton interface of coral carried out by Tambutté et al.(2007). Cellular physiologies and functions (i.e., biomineralization) are generally associated with their morphology (Tambutté et al. 2007; Vandermeulen 1975). Therefore, it is plausible that these two types of cells with morphological differences

394 could have directly/or indirectly controlled the COC and fibers precipitations,
395 respectively.

396 After settlement in stage 2, the calcifying cells may start to exocytose the calcifying
397 precursor and/or medium, which initiates skeletogenesis. It is controversial as to whether
398 the precursor and/or medium is calcium-rich spherules (Tambutté et al. 2007;
399 Vandermeulen 1975), aragonite crystal-bearing vesicles (Hayes and Goreau 1977),
400 amorphous calcium carbonate (Mass et al. 2017; Von Euw et al. 2017), or organic matrix
401 material (Tambutté et al. 2011; Weiner and Dove 2003). The process of cellular
402 exocytosis may occur simultaneously for both types of cells, but each of their secretory
403 products which could influence morphology and chemistry of carbonates (Albeck et al.
404 1996; Chen et al. 2011; Fang et al. 2023; Teng and Dove 1997), are specialized and
405 distinct, which can be inferred from the differences in chemical compositions between the
406 COC and fibers. Additionally, both the intrinsic diurnal growth of the cells (i.e., cell
407 division and diurnal contraction–expansion (Gladfelter 1983b; Raz-Bahat et al. 2006))
408 and extrinsic factors (i.e., the temperature and diurnal cycle in feeding (Constantz 1986;
409 Gladfelter 1983b)) might determine the diurnal secretionary activities, which result in the
410 relatively thin–long filaments and thick–short nodules being deposited during daytime
411 and nighttime, respectively. Such diurnal accretion patterns were not observed in the
412 fibers, which may be due to the relatively low viscosity of the mineralizing matrix either
413 secreted by its calcifying cells or controlled by other mechanisms as compared with that
414 of COC, or different mineralogical/geochemical conditions, i.e., lower crystal growth
415 rates of fiber than that of COC (Cohen et al. 2009b; Sunagawa 2007). The COC are all in
416 intimate physical contact with fibers, which might offer indirect evidence to support that
417 the low viscosity of fiber material and unobservable diurnal patterns of fibers. The
418 compositional differences between the fibers (water-rich) and COC (organic-rich) might
419 contribute to their distinct viscosities, and facilitate the direct physical contact between
420 the COC and fibers, and restrict lateral movement of the COC components.

In the third stage, cell proliferation might increase the population of filaments and nodules and, given that the formation of each filament or nodule is controlled by an individual cell, this would cause COC branching dependent on the increase in cell numbers. In addition, interdigitating cells that overlap are common (Clode and Marshall 2002; Clode and Marshall 2003), which would cause their individual secretions to also overlap. Cells coordination controlled by the transfer and receipt of feedback molecular signals might lead to the formation of multiple COC with quasi-parallel and/or radial patterns in the individual skeleton.

This model highlights the spatiotemporal evolution of skeletogenesis based on calcifying cellular activities and their associated secretions. The three cellular stages may continue throughout the life of an individual coral, which ultimately leads to construction of a coral skeleton. Compared with previous study regarding the ultrastructures of coral skeleton based on SEM examination of acid-etched skeletal surface morphologies (Sugiura et al. 2021), our work combined 3D Raman imaging and CPRL images (with avoidance of possible surface modification or contamination during samples pretreatments) to unprecedentedly reveal ultrastructural distribution and growth features (especially COC which has not been completely visible previously) as well as chemical spatial distribution within the volume of skeleton, which benefits to gain more detailed and comprehensive insight into the possible biological control on skeletal ultrastructural growth. To further ascertain this possible model, additional work, especially interdisciplinary researches, e.g., cytobiology about the linkage of in vivo cells and coral ultrastructures will be needed.

Implications

A combination of Raman spectral imaging and cross-polarized reflected light microscopy imaging is an innovative approach to reveal the three-dimensional spatial distribution, arrangement of skeletal ultrastructures and their associated mineral and

organic compositions within coral, which has never been reported previously and will provide a new perspective for studies on biocarbonate microstructure and biomineralization process.

The important contributions of this work are the development of innovative research methods to gain insight into fine microstructures within biogenic carbonate, and the complement and further modification to the existing calcification mechanism models of coral, which may facilitate exploration in coral-based high temporal resolution such as daily or even diurnal paleoenvironmental reconstruction. Additionally, this work, from a cellular perspective, could also be beneficial to understand the response and adaptation of corals to climatic changes, which may lead to possible protection strategies for coral reefs.

Acknowledgement

The English of the manuscript was improved by Stallard Scientific Editing. This work was supported by the National Natural Sciences Foundation of China (42273012 and 42241104, and 42021002), the Strategic Priority Research Program of Chinese Academy of Sciences (XDB40010300). The data for this paper are available on Zenodo (doi.org/10.5281/zenodo.5558356). The authors have no conflict of interest to declare. This is contribution IS-XXXX from GIGCAS.

References

Akiva, A., Neder, M., Kahil, K., Gavriel, R., and Mass, T. (2018) Minerals in the pre-settled coral Stylophora pistillata crystallize via protein and ion changes. Nature Communications, 9(1).

Al-Horani, F.A., Al-Moghrabi, S.M., and de Beer, D. (2003) The mechanism of calcification and its relation to photosynthesis and respiration in the scleractinian coral Galaxea fascicularis. Marine Biology, 142(3), 419-426.

Albeck, S., Weiner, S., and Addadi, L. (1996) Polysaccharides of Intracrystalline Glycoproteins Modulate Calcite Crystal Growth In Vitro. Chemistry-A European Journal, 2(3), 278-284.

Allemand, D., Tambutté, É., Zoccola, D., and Tambutté, S. (2011) Coral Calcification, Cells to Reefs. In Z. Dubinsky, and N. Stambler, Eds. Coral Reefs: An Ecosystem in Transition, p. 119-150. Springer Netherlands, Dordrecht.

Allison, N. (1996) Geochemical anomalies in coral skeletons and their possible implications for palaeoenvironmental analyses. Marine Chemistry, 55(3), 367-379.

Barnes, D.J., and Yonge, M. (1972) The structure and formation of growth-ridges in scleractinian coral skeletons. Proceedings of the Royal Society of London A, 182(1068), 331-350.

Boon, M., Rickard, W.D.A., Rohl, A.L., and Jones, F. (2020) Stabilization of Aragonite: Role of Mg2+ and Other Impurity Ions. Crystal Growth & Design, 20(8), 5006-5017.

Brahmi, C., Meibom, A., Smith, D.C., Stolarski, J., Auzoux-Bordenave, S., Nouet, J., Doumenc, D., Djediat, C., and Domart-Coulon, I. (2010) Skeletal growth, ultrastructure and composition of the azooxanthellate scleractinian coral Balanophyllia regia. Coral Reefs, 29(1), p.175-189.

Chen, C.-L., Qi, J., Zuckermann, R.N., and DeYoreo, J.J. (2011) Engineered Biomimetic Polymers as Tunable Agents for Controlling CaCO3 Mineralization. Journal of the American Chemical Society, 133(14), 5214-5217.

Chen, T., Robinson, L., Burke, A., Claxton, L., Hain, M., Li, T., Rae, J., Stewart, J., Knowles, T., Fornari, D., and Harpp, K. (2020) Persistently well-ventilated intermediate-depth ocean through the last deglaciation. Nature Geoscience, 13, 1-6.

Chen, T., Robinson Laura, F., Burke, A., Southon, J., Spooner, P., Morris Paul, J., and Ng Hong, C. (2015) Synchronous centennial abrupt events in the ocean and atmosphere during the last deglaciation. Science, 349(6255), 1537-1541.

Clode, P., and Marshall, A. (2002) Low temperature FESEM of the calcifying interface of a scleractinian coral. Tissue Cell, 34(3), 187-198.

Clode, P.L., and Marshall, A. (2003) Calcium associated with a fibrillar organic matrix in the scleractinian coral Galaxea fascicularis. Protoplasma, 220(3), 153-161.

Cohen, A., and McConnaughey, T. (2003) Geochemical Perspectives on Coral Mineralization. Reviews in Mineralogy & Geochemistry, 54, 151-187.

Cohen, A.L., Layne, G.D., Hart, S.R., and Lobel, P.S. (2001) Kinetic control of skeletal Sr/Ca in a symbiotic coral: Implications for the paleotemperature proxy. Paleoceanography, 16(1), 20-26.

Cohen, A.L., McCorkle, D.C., de Putron, S., Gaetani, G.A., and Rose, K.A. (2009a) Morphological and compositional changes in the skeletons of new coral recruits reared in acidified seawater: Insights into the biomineralization response to ocean acidification. Geochemistry Geophysics Geosystems, 10(7).

-. (2009b) Morphological and compositional changes in the skeletons of new coral recruits reared in acidified seawater: Insights into the biomineralization response to ocean acidification. Geochemistry Geophysics Geosystems, 10(7).

Cohen, A.L., and Thorrold, S.R. (2007) Recovery of temperature records from slow-growing corals by fine scale sampling of skeletons. Geophysical Research Letters, 34(17), L17706.

Constantz, B., and Meike, A. (1989) Calcite Centers of Calcification in Mussa Angulosa (Scleractinia). Origin, Evolution, and Modern Aspects of Biomineralization in Plants and Animals.

Constantz, B.R. (1986) Coral skeleton construction: a physiochemically dominated process. Palaios, 152-157.

Cuif, J.-P., and Dauphin, Y. (1998) Microstructural and physico-chemical characterization of ‘centers

of calcification' in septa of some Recent scleractinian corals. Paläontologische Zeitschrift, 72(3), 257-269.

Cuif, J.-P., Dauphin, Y., Berthet, P., and Jegoudez, J. (2004) Associated water and organic compounds in coral skeletons: Quantitative thermogravimetry coupled to infrared absorption spectrometry. Geochemistry Geophysics Geosystems, 5(11).

Cuif, J.P., and Dauphin, Y. (2005a) The Environment Recording Unit in coral skeletons – a synthesis of structural and chemical evidences for a biochemically driven, stepping-growth process in fibres. Biogeosciences, 2(1), 61-73.

-. (2005b) The two-step mode of growth in the scleractinian coral skeletons from the micrometre to the overall scale. Journal of Structural Biology, 150(3), 319-331.

Cuif, J.P., Dauphin, Y., Doucet, J., Salome, M., and Susini, J. (2003) XANES mapping of organic sulfate in three scleractinian coral skeletons. Geochimica et Cosmochimica Acta, 67(1), 75-83.

Cusack, M., and Freer, A. (2008) Biomineralization: Elemental and Organic Influence in Carbonate Systems. Chemical Reviews, 108(11), 4433-4454.

Dauphin, Y. (2001) Comparative studies of skeletal soluble matrices from some Scleractinian corals and Molluscs. International Journal of Biological Macromolecules, 28(4), 293-304.

DeCarlo, T.M. (2018) Characterizing coral skeleton mineralogy with Raman spectroscopy. Nature Communications, 9(1), 5325.

DeCarlo, T.M., Comeau, S., Cornwall, C.E., Gajdzik, L., Guagliardo, P., Sadekov, A., Thillainath, E.C., Trotter, J., and Mcculloch, M.T. (2019a) Investigating marine bio-calcification mechanisms in a changing ocean with in vivo and high-resolution ex vivo Raman spectroscopy. Global Change Biology

DeCarlo, T.M., D'Olivo, J.P., Foster, T., Holcomb, M., Becker, T., and McCulloch, M.T. (2017) Coral calcifying fluid aragonite saturation states derived from Raman spectroscopy. Biogeosciences, 14(22), 5253-5269.

DeCarlo, T.M., Ren, H., and Farfan, G.A. (2018) The Origin and Role of Organic Matrix in Coral Calcification: Insights From Comparing Coral Skeleton and Abiogenic Aragonite. Frontiers in Marine Science, 5, 170.

DeCarlo, T.M., Ross, C.L., and McCulloch, M.T. (2019b) Diurnal cycles of coral calcifying fluid aragonite saturation state. Marine Biology, 166(3), 28.

Dieing, T., Hollricher, O., and Toporski, J. (2011) Confocal Raman Microscopy. Springer.

Domart-Coulon, I., Stolarski, J., Brahmi, C., Gutner-Hoch, E., Janiszewska, K., Shemesh, A., and Meibom, A. (2014) Simultaneous extension of both basic microstructural components in scleractinian coral skeleton during night and daytime, visualized by in situ 86Sr pulse labeling. Journal of Structural Biology, 185(1), 79-88.

Domart-Coulon Isabelle, J., Elbert David, C., Scully Erik, P., Calimlim Precilia, S., and Ostrander Gary, K. (2001) Aragonite crystallization in primary cell cultures of multicellular isolates from a hard coral, Pocillopora damicornis. Proceedings of the National Academy of Sciences, 98(21), 11885-11890.

Falini, G., Fermani, S., and Goffredo, S. (2015) Coral biomineralization: A focus on intra-skeletal

organic matrix and calcification. Seminars In Cell & Developmental Biology, 46, 17-26.

Fang, Y., Lee, S., Xu, H., and Farfan, G.A. (2023) Organic Controls over Biomineral Ca–Mg Carbonate Compositions and Morphologies. Crystal Growth & Design, 23(7), 4872-4882.

Farfan, G.A., Apprill, A., Cohen, A., DeCarlo, T.M., Post, J.E., Waller, R.G., and Hansel, C.M. (2022) Crystallographic and chemical signatures in coral skeletal aragonite. Coral Reefs, 41(1), 19-34.

Farfan, G.A., Apprill, A., Webb, S.M., and Hansel, C.M. (2018a) Coupled X-ray Fluorescence and X-ray Absorption Spectroscopy for Microscale Imaging and Identification of Sulfur Species within Tissues and Skeletons of Scleractinian Corals. Analytical Chemistry, 90(21), 12559-12566.

Farfan, G.A., Cordes, E.E., Waller, R.G., DeCarlo, T.M., and Hansel, C.M. (2018b) Mineralogy of Deep-Sea Coral Aragonites as a Function of Aragonite Saturation State. Frontiers in Marine Science, 5.

Farfan, G.A., Zhou, C., Valley, J.W., and Orland, I.J. (2021) Coupling Mineralogy and Oxygen Isotopes to Seasonal Environmental Shifts Recorded in Modern Freshwater Pearl Nacre From Kentucky Lake. Geochemistry Geophysics Geosystems, 22(12), e2021GC009995.

Gaffey, S.J. (1988) Water in skeletal carbonates. Journal of Sedimentary Research, 58(3), 397-414.

Georgiou, L., Falter, J., Trotter, J., Kline, D.I., Holcomb, M., Dove, S.G., Hoegh-Guldberg, O., and McCulloch, M. (2015) pH homeostasis during coral calcification in a free ocean CO2 enrichment (FOCE) experiment, Heron Island reef flat, Great Barrier Reef. Proceedings of the National Academy of Sciences, 112(43), 13219-13224.

Gilis, M., Meibom, A., Alexander, D., Grauby, O., Stolarski, J., and Baronnet, A. (2015) Morphology, microstructure, crystallography, and chemistry of distinct CaCO3 deposits formed by early recruits of the scleractinian coral Pocillopora damicornis. Journal of Morphology, 276(10), 1146-1156.

Gladfelter, E.H. (1982) Skeletal development in Acropora cervicornis: I. Patterns of calcium carbonate accretion in the axial corallite. Coral Reefs, 1(1), 45-51.

-. (1983a) Skeletal development in Acropora cervicornis - II. Diel patterns of calcium carbonate accretion. Coral Reefs, 2(2), 91-100.

Gladfelter, E.H. (1983b) Spatial and temporal patterns of mitosis in the cells of the axial polyp of the reef coral Acropora cervicornis. Biological Bulletin, 165(3), 811-815.

Hayes, R.L., and Goreau, N.I. (1977) Intracellular Crystal-Bearing Vesicles in the Epidermis of 585 Scleractinian Corals, Astrangia danae (Agassiz) and Porites porites (Pallas). Biological Bulletin, 152(1), 26-40.

He, M., Meng, Y., Yan, S., Hang, W., Zhou, W., and Huang, B. (2017) Three-Dimensional Elemental Imaging of Nantan Meteorite via Femtosecond Laser Ionization Time-of-Flight Mass Spectrometry. Analytical Chemistry, 89(1), 565-570.

Hennige, S.J., Wicks, L.C., Kamenos, N.A., Perna, G., Findlay, H.S., and Roberts, J.M. (2015) Hidden impacts of ocean acidification to live and dead coral framework. Proceedings of The Royal Society B-biological Sciences, 282(1813), 20150990.

Higuchi, T., Fujimura, H., Yuyama, I., Harii, S., Agostini, S., and Oomori, T. (2014) Biotic Control of

Skeletal Growth by Scleractinian Corals in Aragonite–Calcite Seas. PLOS ONE, 9(3), e91021.

Hild, S., Marti, O., and Ziegler, A. (2008) Spatial distribution of calcite and amorphous calcium carbonate in the cuticle of the terrestrial crustaceans Porcellio scaber and Armadillidium vulgare. Journal of Structural Biology, 163(1), 100-108.

Holcomb, M., Cohen, A.L., Gabitov, R.I., and Hutter, J.L. (2009) Compositional and morphological features of aragonite precipitated experimentally from seawater and biogenically by corals. Geochimica et Cosmochimica Acta, 73(14), 4166-4179.

Huang, R.F., Zhang, B.C., Zou, D.X., Hang, W., He, J., and Huang, B.L. (2011) Elemental imaging via laser ionization orthogonal time-of-flight mass spectrometry. Analytical Chemistry, 83(3), 1102-1107.

Lecointe, A., Cohen, S., Gèze, M., Djediat, C., Meibom, A., and Domart-Coulon, I. (2013) Scleractinian coral cell proliferation is reduced in primary culture of suspended multicellular aggregates compared to polyps. Cytotechnology, 65(5), 705-724.

Mann, S. (2001) Biomineralization: principles and concepts in bioinorganic materials chemistry. Oxford University Press on Demand.

Mass, T., Drake, J.L., Haramaty, L., Rosenthal, Y., Schofield, O.M., Sherrell, R.M., and Falkowski, P.G. (2012) Aragonite precipitation by “proto-polyps” in coral cell cultures. PLoS One, 7(4), e35049.

Mass, T., Giuffre, A.J., Sun, C.-Y., Stifler, C.A., Frazier, M.J., Neder, M., Tamura, N., Stan, C.V., Marcus, M.A., and Gilbert, P.U. (2017) Amorphous calcium carbonate particles form coral skeletons. Proceedings of the National Academy of Sciences, 114(37), E7670-E7678.

McCulloch, M., Falter, J., Trotter, J., and Montagna, P. (2012) Coral resilience to ocean acidification and global warming through pH up-regulation. Nature Climate Change, 2(8), 623-627.

Meibom, A., Cuif, J.-P., Houlbreque, F., Mostefaoui, S., Dauphin, Y., Meibom, K.L., and Dunbar, R. (2008) Compositional variations at ultra-structure length scales in coral skeleton. Geochimica et Cosmochimica Acta, 72(6), 1555-1569.

Meibom, A., Mostefaoui, S., Cuif, J.-P., Dauphin, Y., Houlbreque, F., Dunbar, R., and Constantz, B. (2007) Biological forcing controls the chemistry of reef-building coral skeleton. Geophysical Research Letters, 34(2), L02601.

Meibom, A., Stage, M., Wooden, J., Constantz, B.R., Dunbar, R.B., Owen, A., Grumet, N., Bacon, C.R., and Chamberlain, C.P. (2003) Monthly strontium/calcium oscillations in symbiotic coral aragonite: biological effects limiting the precision of the paleotemperature proxy. Geophysical Research Letters, 30(7), 71/1-71/4.

Meibom, A., Yurimoto, H., Cuif, J.P., Domart-Coulon, I., Houlbreque, F., Constantz, B., Dauphin, Y., Tambutté, E., Tambutté, S., and Allemand, D. (2006) Vital effects in coral skeletal composition display strict three-dimensional control. Geophysical Research Letters, 33(11), L11608.

Meldrum, F.C. (2003) Calcium carbonate in biomineralisation and biomimetic chemistry. International Materials Reviews, 48(3), 187-224.

Motai, S., Nagai, T., Sowa, K., Watanabe, T., Sakamoto, N., Yurimoto, H., and Kawano, J. (2012)

Needle-like grains across growth lines in the coral skeleton of Porites lobata. Journal of Structural Biology, 180(3), 389-393.

Otter, L.M. (2019) Micro- to nano-scale architecture and aspects of skeletal growth in marine calcifiers. Sydney, Australia : Macquarie University.

Otter, L.M., Agbaje, O.B.A., Kilburn, M.R., Lenz, C., Henry, H., Trimby, P., Hoppe, P., and Jacob, D.E. (2019) Insights into architecture, growth dynamics, and biomineralization from pulsed Sr-labelled Katelysia rhytiphora shells (Mollusca, Bivalvia). Biogeosciences, 16(17), 3439-3455.

Raz-Bahat, M., Erez, J., and Rinkevich, B. (2006) In vivo light-microscopic documentation for primary calcification processes in the hermatypic coral Stylophora pistillata. Cell And Tissue Research, 325(2), 361-368.

Risk, M.J., and Pearce, T.H. (1992) Interference imaging of daily growth bands in massive corals. Nature, 358(6387), 572-573.

Stolarski, J. (2003) Three-dimensional micro- and nanostructural characteristics of the scleractinian coral skeleton: A biocalcification proxy. Acta Palaeontologica Polonica, 48, 497-530.

Sugiura, M., Yasumoto, K., Iijima, M., Oaki, Y., and Imai, H. (2021) Morphological study of fibrous aragonite in the skeletal framework of a stony coral. CrystEngComm, 23(20), 3693-3700.

Sunagawa, I. (2007) Crystals: growth, morphology, & perfection. Cambridge University Press.

Tambutté, E., Allemand, D., Zoccola, D., Meibom, A., Lotto, S., Caminiti, N., and Tambutté, S. (2007) Observations of the tissue-skeleton interface in the scleractinian coral Stylophora pistillata. Coral Reefs, 26(3), 517-529.

Tambutté, E., Venn, A., Holcomb, M., Segonds, N., Techer, N., Zoccola, D., Allemand, D., and Tambutté, S. (2015) Morphological plasticity of the coral skeleton under CO 2-driven seawater acidification. Nature Communications, 6, 7368.

Tambutté, S., Holcomb, M., Ferrier-Pagès, C., Reynaud, S., Tambutté, É., Zoccola, D., and Allemand, D. (2011) Coral biomineralization: From the gene to the environment. Journal of Experimental Marine Biology and Ecology, 408, 58-78.

Teng, H.H., and Dove, P.M. (1997) Surface site-specific interactions of aspartate with calcite during dissolution: Implications for biomineralization. American Mineralogist, 82(9-10), 878-887.

Thompson, D.M. (2022) Environmental records from coral skeletons: A decade of novel insights and innovation. Wiley Interdisciplinary Reviews-climate Change, 13(1), e745.

Tissier, M.D.A.A.L. (1988) Diurnal patterns of skeleton formation in Pocillopora damicornis (Linnaeus). Coral Reefs, 7(2), 81-88.

Urmos, J., Sharma, S.K., and Mackenzie, F.T. (1991) Characterization of some biogenic carbonates with Raman spectroscopy. American Mineralogist, 76(3-4), 641-646.

Vandermeulen, J.H. (1975) Studies on reef corals. III. Fine structural changes of calicoblast cells in Pocillopora damicornis during settling and calcification. Marine Biology, 31(1), 69-77.

Von Euw, S., Zhang, Q., Manichev, V., Murali, N., Gross, J., Feldman, L.C., Gustafsson, T., Flach, C., Mendelsohn, R., and Falkowski, P.G. (2017) Biological control of aragonite formation in stony corals. Science, 356(6341), 933-938.

Wall, M., and Nehrke, G. (2012) Reconstructing skeletal fiber arrangement and growth mode in the

coral *Porites lutea* (Cnidaria, Scleractinia): a confocal Raman microscopy study. Biogeosciences, 9(11), 4885-4895.

Weiner, S., and Dove, P.M. (2003) An overview of biomineralization processes and the problem of the vital effect. Reviews in Mineralogy & Geochemistry, 54(1), 1-29.

Weiner, S., Levi-Kalisman, Y., Raz, S., and Addadi, L. (2003) Biologically formed amorphous calcium carbonate. Connective Tissue Research, 44(1), 214-218.

Yan, H., Liu, C., An, Z., Yang, W., Yang, Y., Huang, P., Qiu, S., Zhou, P., Zhao, N., Fei, H., Ma, X., Shi, G., Dodson, J., Hao, J., Yu, K., Wei, G., Yang, Y., Jin, Z., and Zhou, W. (2020) Extreme weather events recorded by daily to hourly resolution biogeochemical proxies of marine giant clam shells. Proceedings of the National Academy of Sciences, 117(13), 7038-7043.

Zhang, F., Cai, W., Zhu, J., Sun, Z., and Zhang, J. (2011) In situ raman spectral mapping study on the microscale fibers in blue coral (Heliopora coerulea) skeletons. Analytical Chemistry, 83(20), 7870-5.

Zou, J., Deng, W., Chen, X., Liu, X., Guo, Y., Cai, G., Xia, X., Yang, Q., Zhang, Y., Zeng, T., and Wei, G. (2021) Temperature control on high-resolution SIMS oxygen isotopic compositions in Porites coral skeletons. Solid Earth Sciences, 6(2), 129-141.

This is the peer-reviewed, final accepted version for American Mineralogist, published by the Mineralogical Society of America.
The published version is subject to change. Cite as Authors (Year) Title. American Mineralogist, in press.
DOI: https://doi.org/10.2138/am-2023-9134. http://www.minsocam.org/

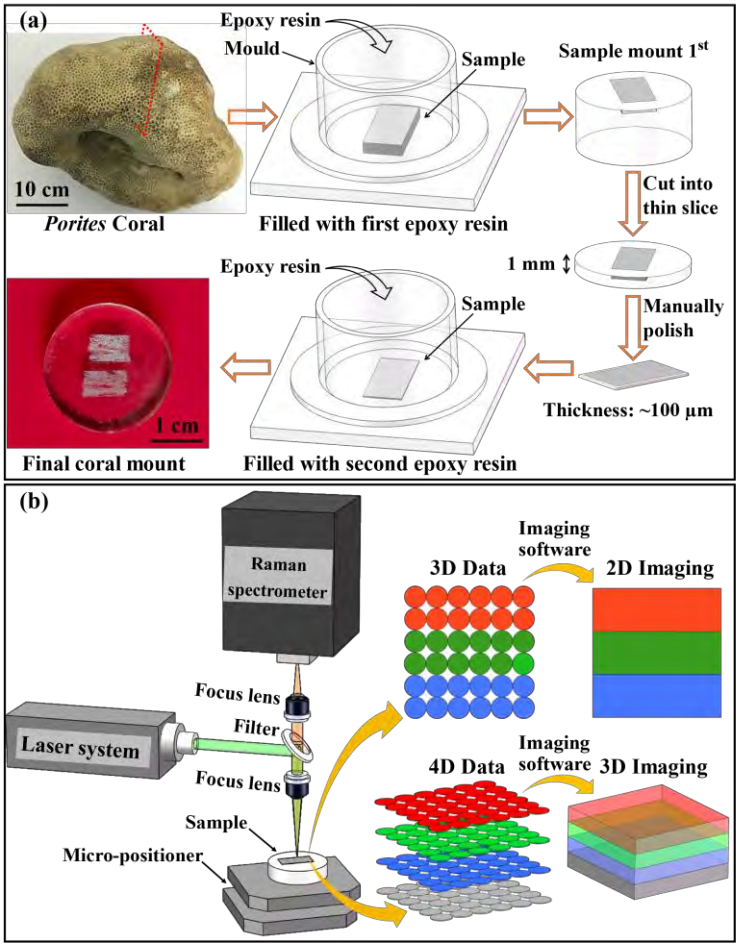

Fig. 1 (a) Sample preparation procedure based on a previous study (Zou et al. 2021). (b) Schematic diagram of the Raman spectroscopy system and imaging procedure.

This is the peer-reviewed, final accepted version for American Mineralogist, published by the Mineralogical Society of America.
The published version is subject to change. Cite as Authors (Year) Title. American Mineralogist, in press.
DOI: https://doi.org/10.2138/am-2023-9134. http://www.minsocam.org/

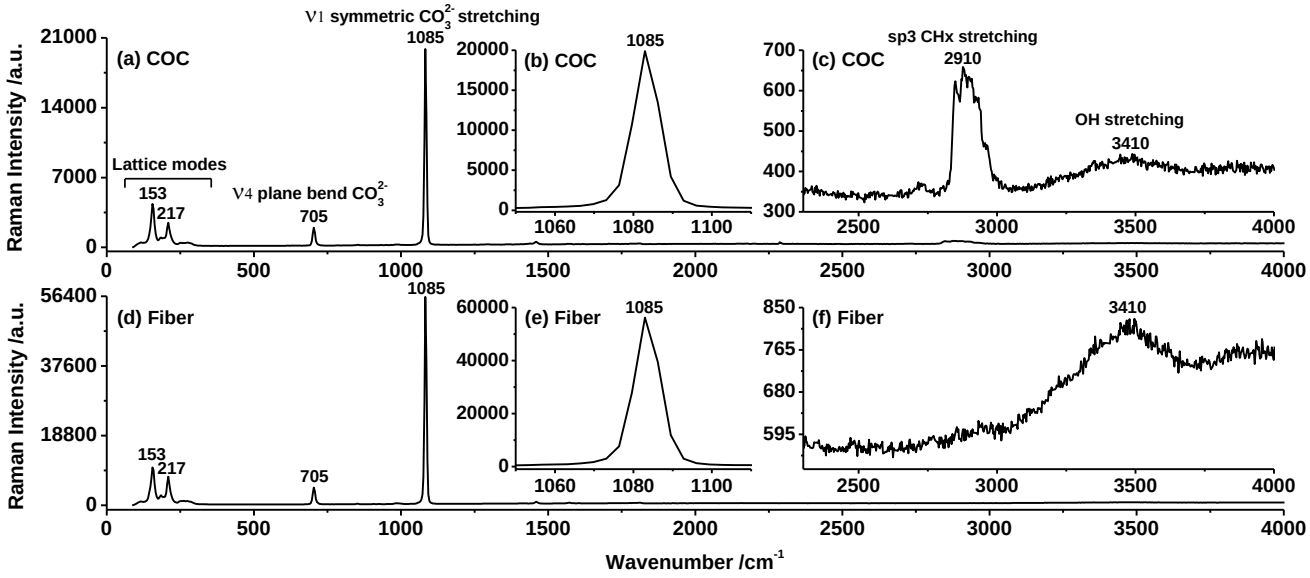

Fig. 2 Typical Raman spectra for (a–c) COC, where (b) and (c) are enlarged views of parts of (a); and (d–f) fibers, where (e) and (f) are enlarged views of parts of (d). An integration time of 10 s was applied in acquiring spectra for both the COC and fibers.

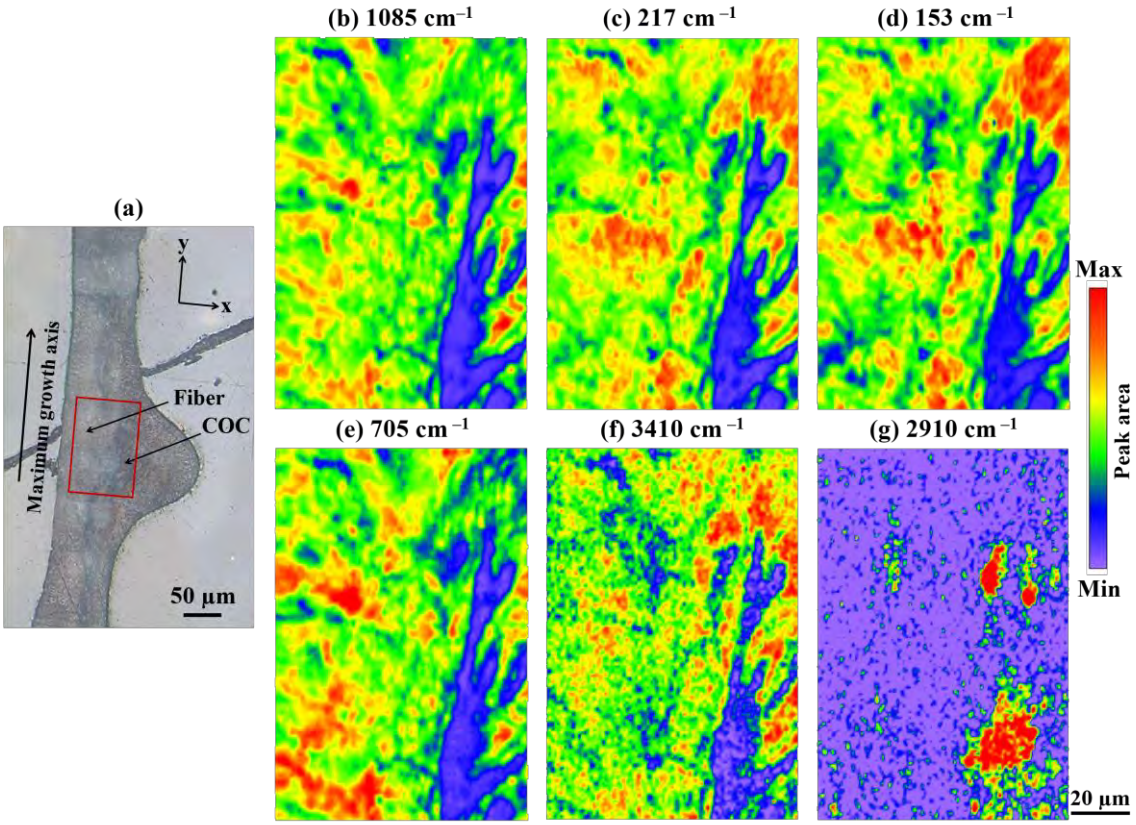

712 **Fig. 3** Two-dimensional images of the coral skeleton over an 85×125 μm area. (a)
713 Reflected-light microscopic image; and (b–g) images obtained from the 1085, 217, 153,
714 705, 3410, and 2910 cm^{-1} Raman bands, respectively.
715

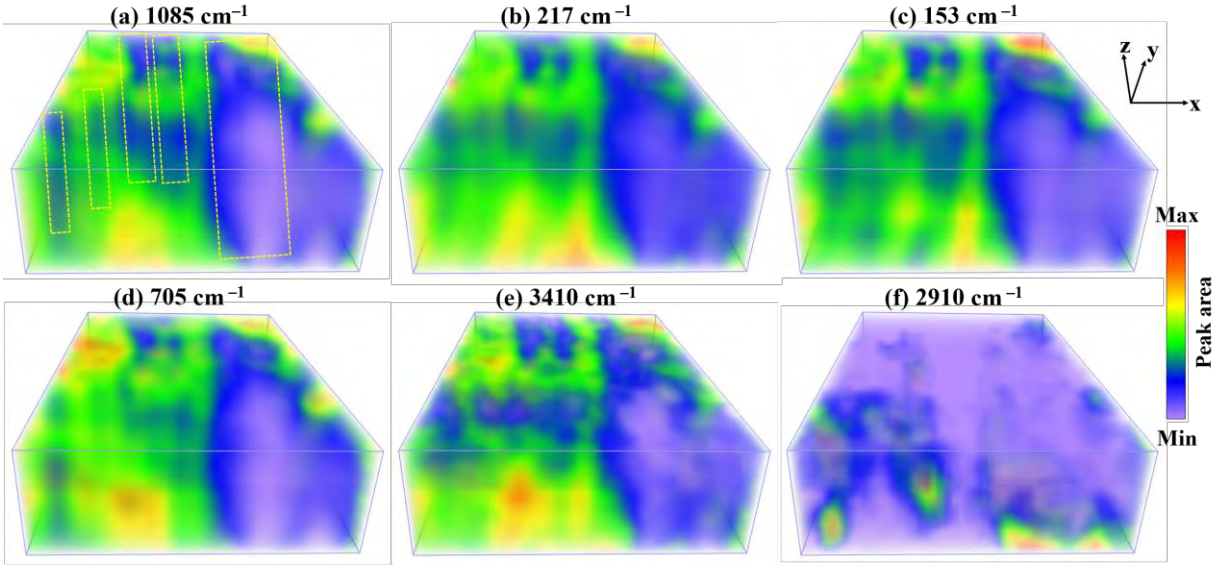

716
717 **Fig. 4** (a–f) Three-dimensional Raman imaging of the Raman bands at 1085, 217, 153,
718 705, 3410, and 2910 cm^{-1} in the coral skeleton. The imaged area is the same as that of the
719 two-dimensional imaging (Fig. 2). Blue–purple regions in (a–e) correspond to the COC,
720 and the yellow dotted rectangles indicate the parallel columns of COC.
721

This is the peer-reviewed, final accepted version for American Mineralogist, published by the Mineralogical Society of America.
The published version is subject to change. Cite as Authors (Year) Title. American Mineralogist, in press.
DOI: https://doi.org/10.2138/am-2023-9134. http://www.minsocam.org/

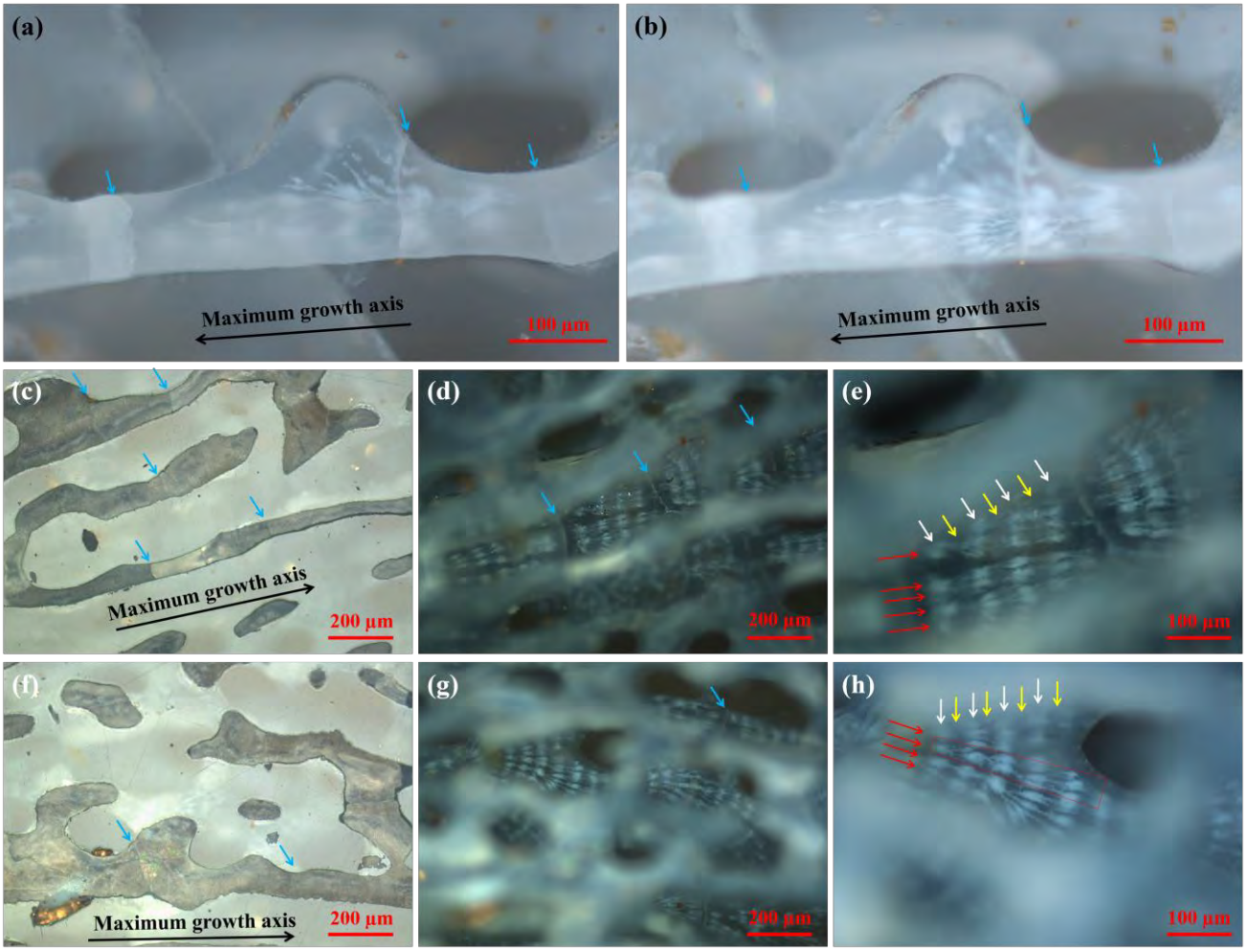

Fig. 5 Optical microscopy images of the section of *Porites* coral skeleton. (a–b) Cross-polarized reflected light (CPRL) microscopy images of the same area imaged by Raman spectroscopy at different focusing depths; (c–h) Optical and CPRL microscopy images of two different sections of the sub-surfaced skeleton. (c) and (f) are optical microscopy images of the coral skeleton embedded in epoxy resin. (d–e) and (g–h) are CPRL microscopy images, with (e) and (h) being higher-magnification views of (d) and (g). The blue, white, yellow and red arrows indicate the fractures, nodules, filaments, and COC columns, respectively. And the dotted trapezoid indicates that the nodules changes with skeletal growth within an individual COC column.

This is the peer-reviewed, final accepted version for American Mineralogist, published by the Mineralogical Society of America.
The published version is subject to change. Cite as Authors (Year) Title. American Mineralogist, in press.
DOI: https://doi.org/10.2138/am-2023-9134. http://www.minsocam.org/

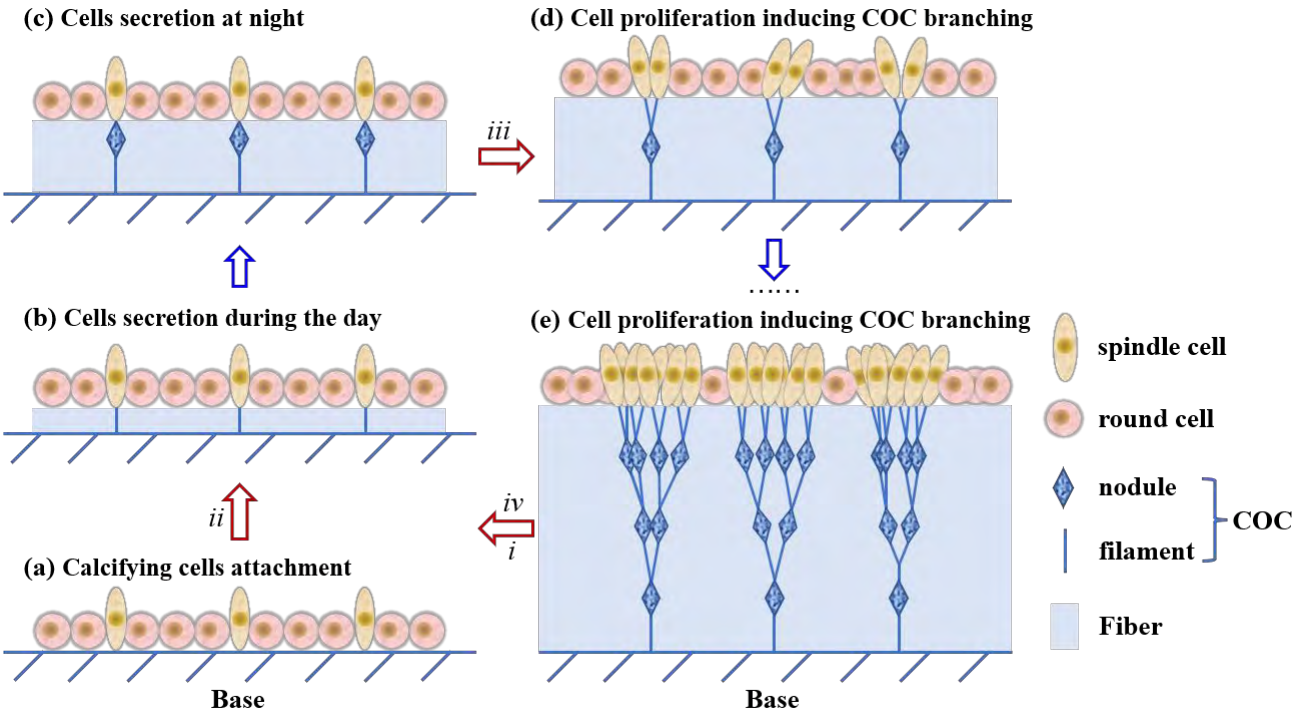

733

734 **Fig. 6** Working model of the process of coral mineralization involving three stages. (a)
735 Attachment of calcifying cells, including round- and spindle-shaped cells. (b–c)
736 Secretions by the round- and spindle-shaped cells form fibers and the COC, respectively.
737 The spindle-shaped cells dominate COC accretion in the form of filaments and nodules in
738 daytime and nighttime, respectively. (d–e) Cell proliferation causes COC branching.

739